Calculation of effective point reactor kinetic parameters combined with the Galerkin finite element method

Bao-Xin Yuan[1,2] [ID] · **Wan-Kui Yang[1]** · **Song-Bao Zhang[1]** · **Bin Zhong[2]** ·
Jun-Xia Wei[2] · **Yang-Jun Ying[2]**

Abstract Precise point reactor kinetic parameters are
essential in the study of reactor dynamics. Point reactor
kinetic parameters include the effective delayed neutron
fraction and prompt neutron lifetime. In this work, effec-
tive point reactor kinetic parameters, which can be applied
to unstructured grids, were calculated based on the Galer-
kin finite element method. First, two-dimensional and
three-dimensional benchmarks were used to verify the
calculation of steady-state neutronic parameters. Then, the
Tehran research reactor core was divided into hexahedral
meshes, and the forward flux and adjoint flux were calcu-
lated. Finally, the effective point reactor kinetic parameters
of the Tehran research reactor were obtained by compre-
hensively processing the steady-state neutronic parameters.

Keywords Finite element method · Reactor · Kinetic
parameters

✉ Bao-Xin Yuan
  bxyuan@caep.cn

[1] Institute of Nuclear Physics and Chemistry, China Academy
   of Engineering Physics, Mianyang 621900, China

[2] Institute of Applied Physics and Computational Mathematics,
   Beijing 100094, China

1 Introduction

The finite element method can handle unstructured
meshes and can thus be adapted to complex geometries.
Since the 1970s, this method has been gradually applied
and promoted in the field of neutronics computing [1–4].

Zhang et al. [5] proposed a strategy to accelerate solving
the neutron diffusion equation via the finite element
method, and the acceleration ratio reached 10^3. Hosseini
et al. [6–9] proposed a finite element method for solving
steady-state neutronics and neutron noise problems.
Avvakumov et al. [10] also solved a typical neutron
dynamics problem via the finite element method. The finite
element platform FEniCS was used to develop the neutron
dynamics code, and the extensible tool package SLEPc was
used to solve the eigenvalue of the coefficient matrix.
González-Pintor et al. [11] proposed a high-order finite
element method to solve the lambda eigenvalue problem of
hexagonal geometry.

For analyzing reactor dynamics, effective point reactor
kinetic parameters need to be obtained in advance, and
finite element methods can be used.

Saadi et al. [12] reviewed the calculation methods of
effective point reactor kinetic parameters and compared
deterministic and stochastic methods by using the same
benchmark. Arkani et al. [13] calculated the effective point
reactor kinetic parameters of the Tehran research reactor
(TRR) by using the six-group weighting method. Lashkari
et al. [14] calculated the effective point reactor kinetic
parameters of the TRR mixed core through the core anal-
ysis tool MTR_PC. The effective delayed neutron fraction
was found to decrease with burnup, while the prompt
neutron lifetime increased. With increasing highly enriched
uranium fuel assemblies, the prompt neutron lifetime

increases, while the effective delayed neutron fraction does not change significantly. Hosseini et al. [15] calculated and measured the effective point reactor kinetic parameters of the TRR. MTR_PC was used to calculate the neutronic parameters of the TRR in cold and hot states. By using WIMS and CITATION, Zaker et al. [16] calculated the effective point reactor kinetic parameters of two TRR cores with both highly enriched uranium and low enriched uranium.

To improve the steady-state calculation in the current deterministic method of effective point reactor kinetic parameters, the calculation of these parameters and the Galerkin finite element method are combined in this work based on the existing framework of FEMN [17]. This paper is organized as follows: the basic concepts of the Galerkin finite element method are outlined, and the 2D and 3D steady-state benchmarks based on the Galerkin finite element method are verified in Sect. 2. In Sect. 3, the TRR benchmarks used worldwide are described, and the effective point reactor kinetic parameters of the TRR are obtained by the improved strategy proposed above. In the final section, the calculation results are discussed, and a brief summary is provided.
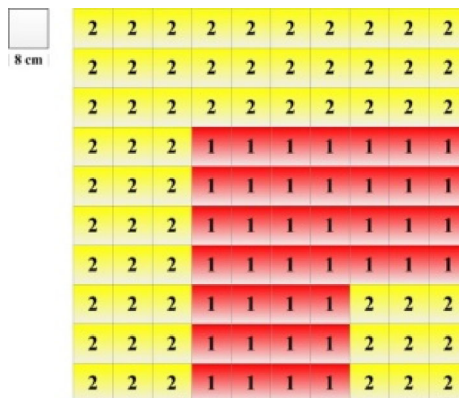
2 Galerkin finite element method

2.1 Galerkin finite element formulation of the neutron diffusion problem

The effective delayed neutron fraction is defined as follows:

$$\beta_i^{\text{eff}} = \frac{\iiint \sum_{g=1}^{G} \emptyset_g^* \chi_{\text{di}}^q \beta_i^q \sum_{g'=1}^{G} \left(v \sum_{\text{f}}\right)_{g'} \emptyset_{g'} \mathrm{d}V}{\iiint \sum_{g=1}^{G} \emptyset_g^* \chi_p^q \sum_{g'=1}^{G} v \Sigma_{\text{f}}^{g'}(\text{r}) \emptyset_{g'} \mathrm{d}V}. \tag{1}$$

For group g, $\emptyset_g^*$ is the adjoint flux, χ_{di}^q is the delayed neutron spectrum of fissionable isotope q in group i, β_i^q is the delayed neutron yield for fissionable isotope q in group i, v is the number of neutrons emitted per fission, $\left(\sum_{\text{f}}\right)_{g'}$ is the fission cross section, $\emptyset_g$ is the forward flux, and χ_p^q is the prompt neutron spectrum of fissionable isotope q.
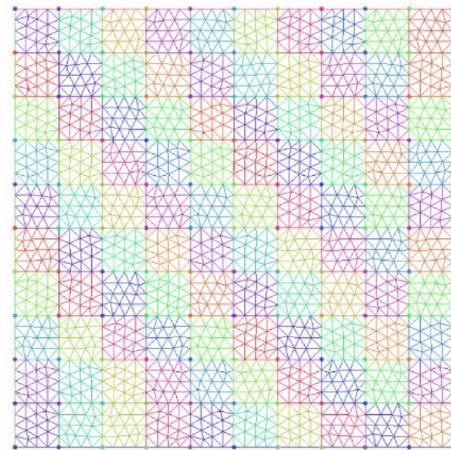
Fig. 2 (Color online) Meshes used by the 2D benchmark

Table 2 k_{eff}^* of TWIGL

Item	Calculated value/reference value (deviation)
k_{eff}^*	1.001312/1.001310 (0.000002)

Fig. 1 (Color online) Schematic of the 2D benchmark

Table 1 Macroscopic cross sections of the TWIGL 2D benchmark

Material types	Energy group	$D_g(\text{cm}^{-1})$	$\sum_{\text{t},g}(\text{cm}^{-1})$	$\left(v\sum_{\text{f}}\right)_g(\text{cm}^{-1})$	$\sum_{g'\rightarrow g}(\text{cm}^{-1})$
1	1	1.4	0.01	0.007657	0.01
	2	0.4	0.15	0.218772	0
2	1	1.3	0.008	0.00328158	0.01
	2	0.5	0.05	0.06563	0

Table 3 Distribution of the fast group adjoint flux for the 2D benchmark obtained by FEMN

0.2138	0.2095	0.2006	0.1866	0.1674	0.1431	0.1164	0.0839	0.0553	0.0238
0.2103	0.2060	0.1972	0.1835	0.1645	0.1405	0.1125	0.0823	0.0520	0.0229
1.62%	1.65%	1.68%	1.68%	1.75%	1.85%	3.39%	1.96%	5.96%	3.92%
0.4910	0.4814	0.4615	0.4301	0.3862	0.3298	0.2631	0.1909	0.1200	0.0533
0.4892	0.4796	0.4596	0.4282	0.3843	0.3281	0.2614	0.1895	0.1186	0.0520
0.37%	0.37%	0.41%	0.44%	0.48%	0.51%	0.63%	0.71%	1.14%	2.43%
0.8132	0.7985	0.7674	0.7173	0.6455	0.5513	0.4365	0.3099	0.1909	0.0839
0.8129	0.7981	0.7669	0.7165	0.6446	0.5503	0.4354	0.3088	0.1895	0.0822
0.04%	0.05%	0.07%	0.11%	0.14%	0.18%	0.26%	0.36%	0.75%	2.02%
1.1600	1.1415	1.1014	1.0344	0.9350	0.8001	0.6305	0.4363	0.2629	0.1145
1.1597	1.1412	1.1009	1.0337	0.9341	0.7990	0.6293	0.4355	0.2615	0.1125
0.02%	0.03%	0.05%	0.07%	0.10%	0.14%	0.19%	0.19%	0.55%	1.78%
1.4239	1.4063	1.3660	1.2935	1.1782	1.0136	0.7998	0.5509	0.3295	0.1429
1.4243	1.4067	1.3663	1.2936	1.1780	1.0131	0.7990	0.5503	0.3280	0.1405
0.03%	0.03%	0.02%	0.01%	0.02%	0.05%	0.10%	0.11%	0.44%	1.68%
1.5655	1.5556	1.5289	1.4693	1.3563	1.1778	0.9344	0.6449	0.3857	0.1672
1.5667	1.5569	1.5302	1.4705	1.3571	1.1781	0.9341	0.6447	0.3843	0.1645
0.08%	0.09%	0.09%	0.08%	0.06%	0.02%	0.03%	0.04%	0.36%	1.62%
1.5634	1.5683	1.5739	1.5566	1.4687	1.2925	1.0334	0.7164	0.4295	0.1864
1.5654	1.5705	1.5762	1.5588	1.4705	1.2936	1.0337	0.7165	0.4282	0.1834
0.12%	0.14%	0.15%	0.14%	0.12%	0.08%	0.03%	0.01%	0.31%	1.59%
1.4381	1.4617	1.5145	1.5731	1.5276	1.3645	1.1000	0.7664	0.4609	0.2003
1.4419	1.4660	1.5191	1.5762	1.5302	1.3663	1.1009	0.7669	0.4596	0.1972
0.27%	0.29%	0.31%	0.19%	0.17%	0.13%	0.08%	0.06%	0.27%	1.54%
1.3344	1.3734	1.4610	1.5668	1.5536	1.4043	1.1398	0.7973	0.4807	0.2092
1.3388	1.3778	1.4660	1.5706	1.5569	1.4067	1.1411	0.7981	0.4796	0.2061
0.29%	0.32%	0.34%	0.24%	0.21%	0.17%	0.12%	0.10%	0.23%	1.50%
1.2871	1.3339	1.4367	1.5613	1.5632	1.4216	1.1582	0.8120	0.4903	0.2135
1.2910	1.3382	1.4419	1.5653	1.5668	1.4243	1.1597	0.8129	0.4892	0.2103
0.30%	0.33%	0.36%	0.26%	0.23%	0.19%	0.13%	0.11%	0.22%	1.18%

—Reference value

—Calculated value

—Deviation %

Similarly, the definition of prompt neutron lifetime can be given as follows:

$$l = \frac{k_{\text{eff}} \iiint \sum_{g=1}^{G} \emptyset_g^* \frac{1}{v_g} \emptyset_g \mathrm{d}V}{\iiint \sum_{g=1}^{G} \emptyset_g^* \chi_i^g \sum_{g'=1}^{G} v\Sigma_{\text{f}}^{g'} \emptyset_{g'} \mathrm{d}V}, \qquad (2)$$

where $\frac{1}{v_g}$ is the inverse velocity of group g.

The 3D steady-state equation of neutronics is as follows:

$$-\nabla \cdot D_g \nabla \emptyset_g + \sum_{\text{r},g} \emptyset_g = \sum_{g'=1}^{G} \sum_{g' \to g} \emptyset_{g'} + \frac{\chi_g}{k_{\text{eff}}} \sum_{g'=1}^{G} \left(v \sum_{\text{f}} \right)_{g'} \emptyset_{g'}. \qquad (3)$$

For group g, D_g is the diffusion coefficient, $\sum_{\text{r},g}$ is the removal cross section, $\sum_{g' \to g}$ is the scattering cross section

from group g' to g, χ_g is the fission spectrum, and k_{eff} is the effective multiplication factor.

The boundary conditions are described as follows:

$$\left(\alpha D_g \frac{\partial \emptyset_g}{\partial n} + \beta \emptyset_g \right)|\Gamma_1 = 0 \quad \alpha \neq 0, \qquad (4)$$

where Γ_1 is the boundary, n is the normal direction of Γ_1, and α and β are constants.

By following the Galerkin finite element method, the weak form of the diffusion equation can be written as follows:

Table 4 Distribution of the thermal group adjoint flux for the 2D benchmark obtained by FEMN

0.2656	0.2603	0.2492	0.2319	0.2080	0.1777	0.1424	0.1042	0.0660	0.0277
0.2612	0.2559	0.2449	0.2278	0.2042	0.1744	0.1397	0.1021	0.0644	0.0266
1.64%	1.70%	1.72%	1.75%	1.81%	1.83%	1.92%	2.02%	2.40%	3.97%
0.6510	0.6384	0.6120	0.5703	0.5120	0.4373	0.3487	0.2528	0.1584	0.0660
0.6486	0.6359	0.6094	0.5677	0.5096	0.4350	0.3465	0.2509	0.1567	0.0644
0.37%	0.40%	0.43%	0.45%	0.48%	0.53%	0.64%	0.74%	1.10%	2.39%
1.0984	1.0785	1.0365	0.9687	0.8718	0.7445	0.5880	0.4130	0.2528	0.1042
1.0933	1.0791	1.0371	0.9689	0.8716	0.7440	0.5872	0.4115	0.2508	0.1020
0.08%	0.06%	0.06%	0.02%	0.03%	0.07%	0.14%	0.37%	0.78%	2.09%
1.6698	1.6432	1.5855	1.4891	1.3460	1.1517	0.9013	0.5878	0.3485	0.1422
1.6683	1.6416	1.5836	1.4870	1.3437	1.1494	0.8985	0.5874	0.3465	0.1396
0.09%	0.10%	0.12%	0.14%	0.17%	0.20%	0.31%	0.07%	0.58%	1.79%
2.0651	2.0395	1.9811	1.8760	1.7089	1.4700	1.1514	0.7440	0.4369	0.1775
2.0650	2.0395	1.9809	1.8755	1.7080	1.4688	1.1494	0.7440	0.4349	0.1745
0.00%	0.00%	0.01%	0.02%	0.05%	0.08%	0.18%	0.00%	0.45%	1.69%
2.2705	2.2561	2.2174	2.1311	1.9672	1.7082	1.3451	0.8710	0.5115	0.2077
2.2715	2.2574	2.2186	2.1321	1.9677	1.7081	1.3438	0.8716	0.5095	0.2043
0.04%	0.06%	0.06%	0.05%	0.03%	0.01%	0.01%	0.07%	0.39%	1.63%
2.2515	2.2588	2.2698	2.2559	2.1302	1.8746	1.4876	0.9676	0.5695	0.2316
2.2527	2.2604	2.2716	2.2586	2.1322	1.8756	1.4870	0.9688	0.5677	0.2278
0.05%	0.07%	0.08%	0.12%	0.09%	0.05%	0.04%	0.12%	0.32%	1.63%
1.9432	1.9767	2.0742	2.2687	2.2154	1.9789	1.5835	1.0351	0.6111	0.2488
1.9501	1.9840	2.0840	2.2716	2.2186	1.9809	1.5837	1.0370	0.6094	0.2449
0.36%	0.37%	0.47%	0.13%	0.15%	0.10%	0.01%	0.18%	0.28%	1.57%
1.7717	1.8258	1.9756	2.2566	2.2532	2.0366	1.6408	1.0769	0.6374	0.2599
1.7762	1.8310	1.9841	2.2604	2.2573	2.0396	1.6415	1.0793	0.6359	0.2559
0.26%	0.28%	0.43%	0.17%	0.18%	0.14%	0.04%	0.23%	0.24%	1.55%
1.7066	1.7710	1.9414	2.2484	2.2670	2.0617	1.6672	1.0967	0.6501	0.2652
1.7112	1.7762	1.9500	2.2527	2.2716	2.0651	1.6682	1.0993	0.6486	0.2612
0.27%	0.29%	0.44%	0.19%	0.20%	0.17%	0.06%	0.24%	0.23%	1.51%

—Reference value

—Calculated value

—Deviation %

(a)

(b)
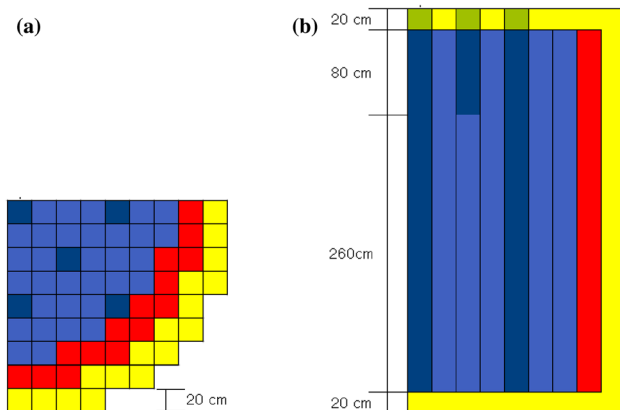
Fig. 3 (Color online) Schematic of the 3D benchmark. **a** top view; **b** side view

$$\iiint_{\Omega} -v\nabla \cdot D_g \nabla \emptyset_g \mathrm{d}V$$

$$+ \iiint_{\Omega} v \sum_{\mathrm{r},g} \emptyset_g \mathrm{d}V = \iiint_{\Omega} v \sum_{g'=1}^{G} \sum_{g' \to g} \emptyset_{g'} \mathrm{d}V \tag{5}$$

$$+ \iiint_{\Omega} v \frac{\chi_g}{k_{\mathrm{eff}}} \sum_{g'=1}^{G} \left(v \sum_{\mathrm{f}} \right)_{g'} \emptyset_{g'} \mathrm{d}V.$$

After integration by parts, the finite element form of the 3D steady-state neutronics equation can be obtained:

Table 5 Macroscopic cross sections of the IAEA 3D benchmark

	Material types	Energy group	$D_g(\mathrm{cm}^{-1})$	$\sum_{t,g}(\mathrm{cm}^{-1})$	$(v\sum_f)_g(\mathrm{cm}^{-1})$	$\sum_{g\to g'}(\mathrm{cm}^{-1})$
	Fuel1	1	1.500	0.010	0.000	0.020
		2	0.400	0.085	0.135	–
	Fuel1 + rod	1	1.500	0.010	0.000	0.020
		2	0.400	0.130	0.135	–
	Fuel2	1	1.500	0.010	0.000	0.020
		2	0.400	0.080	0.135	–
	Reflector	1	2.000	0.000	0.000	0.040
		2	0.300	0.010	0.000	–
	Reflector + Rod	1	2.000	0.000	0.000	0.040
		2	0.300	0.055	0.000	–

Fig. 4 (Color online) Meshes used by the IAEA 3D benchmark
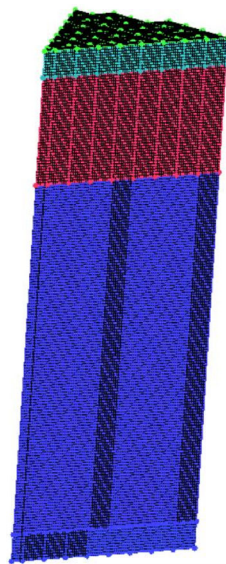
Table 6 k_{eff} and k_{eff}^* of IAEA-3D PWR

Item	Value
Reference k_{eff}	1.02900
Calculated k_{eff}	1.02904
Calculated k_{eff}^*	1.02910

Table 7 Power distribution of the 3D benchmark obtained by FEMN

0.7290					
0.7237					
0.73%					
1.2810	1.3970				
1.2643	1.3802				
1.31%	1.21%				
1.4220	1.4320	1.3680			
1.4068	1.4160	1.3547			
1.07%	1.12%	0.98%			
1.1930	1.2910	1.3110	1.1780		
1.1815	1.2798	1.3019	1.1725		
0.96%	0.87%	0.70%	0.47%		
0.6100	1.0720	1.1810	0.9720	0.4760	
0.6113	1.0663	1.1779	0.9701	0.4794	
0.21%	0.54%	0.26%	0.20%	0.72%	
0.9530	1.0550	1.0890	0.9230	0.7000	0.5970
0.9536	1.0568	1.0923	0.9275	0.7046	0.6093
0.07%	0.17%	0.31%	0.49%	0.65%	2.06%
0.9590	0.9760	1.0000	0.8660	0.6100	
0.9664	0.9829	1.0077	0.8789	0.6233	
0.78%	0.71%	0.77%	1.50%	2.01%	
0.7770	0.7570	0.7110			
0.7896	0.7690	0.7262			
1.62%	1.58%	2.14%			

—Reference value

—Calculated value

—Deviation %

$$\iiint_\Omega D_g \nabla\emptyset_g \cdot \nabla v \mathrm{d}V + \iiint_\Omega v \sum_{r,g}\emptyset_g \mathrm{d}V + \iint_{\Gamma_1}\frac{\beta}{\alpha}\emptyset_g v \mathrm{d}S$$
$$= \iiint_\Omega v \sum_{g'=1}^{G}\sum_{g'\to g}\emptyset_{g'}\mathrm{d}V$$
$$+ \iiint_\Omega v \frac{\chi_g}{k_{\mathrm{eff}}}\sum_{g'=1}^{G}\left(v\sum_f\right)_{g'}\emptyset_{g'}\mathrm{d}V.$$

(6)

The 3D steady-state adjoint equation of neutronics is as follows:

$$-\nabla\cdot D_g\nabla\emptyset_g^* + \sum_{r,g}\emptyset_g^* = \sum_{g'\neq g}\sum_{g\to g'}\emptyset_{g'}^* + \frac{(v\sum_f)_g}{k_{\mathrm{eff}}}\sum_{g'=1}^{G}\chi_{g'}\emptyset_{g'}^*.$$
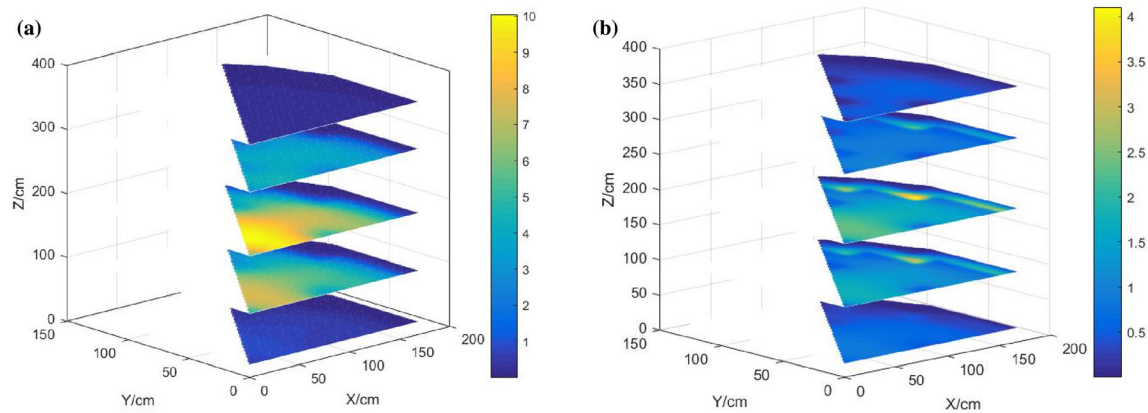
(7)

Fig. 5 (Color online) Distribution of forward flux for the 3D benchmark obtained by FEMN ($Z = 19$ cm, 99 cm, 189 cm, 289 cm, 363 cm). **a** fast group forward flux; **b** thermal group forward flux
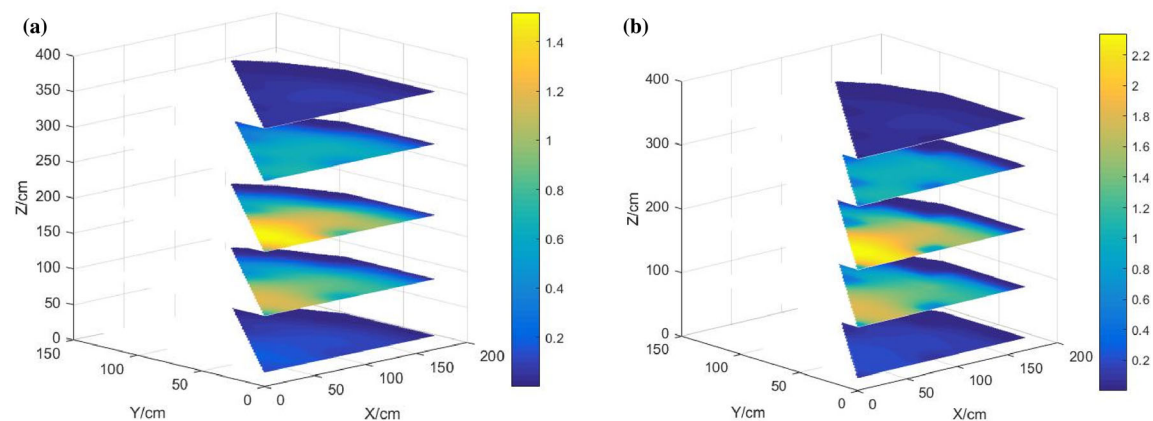

Fig. 6 (Color online) Distribution of adjoint flux for the 3D benchmark obtained by FEMN ($Z = 19$ cm, 99 cm, 189 cm, 289 cm, 363 cm). **a** fast group adjoint flux; **b** thermal group adjoint flux

Similarly, the finite element form of the 3D steady-state neutronics adjoint equation can be obtained as follows:

$$\iiint_\Omega D_g \nabla \emptyset_g^* \cdot \nabla v \mathrm{d}V + \iiint_\Omega v \sum_{\mathrm{r},g} \emptyset_g^* \mathrm{d}V + \iint_{\Gamma_1} \frac{\beta}{\alpha} \emptyset_g^* v \mathrm{d}S$$
$$= \iiint_\Omega v \sum_{g' \neq g}^{G} \sum_{g \to g'} \emptyset_{g'}^* \mathrm{d}V + \iiint_\Omega v \frac{(v \sum_\mathrm{f})_g}{k_{\mathrm{eff}}} \sum_{g'=1}^{G} \chi_{g'} \emptyset_{g'}^* \mathrm{d}V.$$

$$(8)$$

2.2 Benchmark test

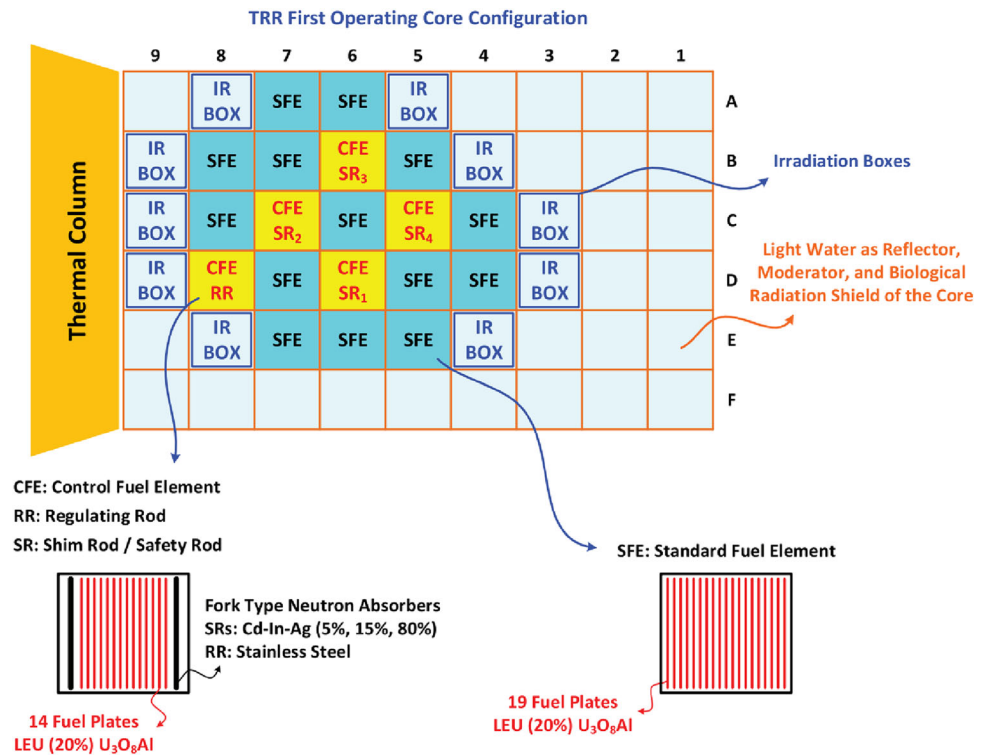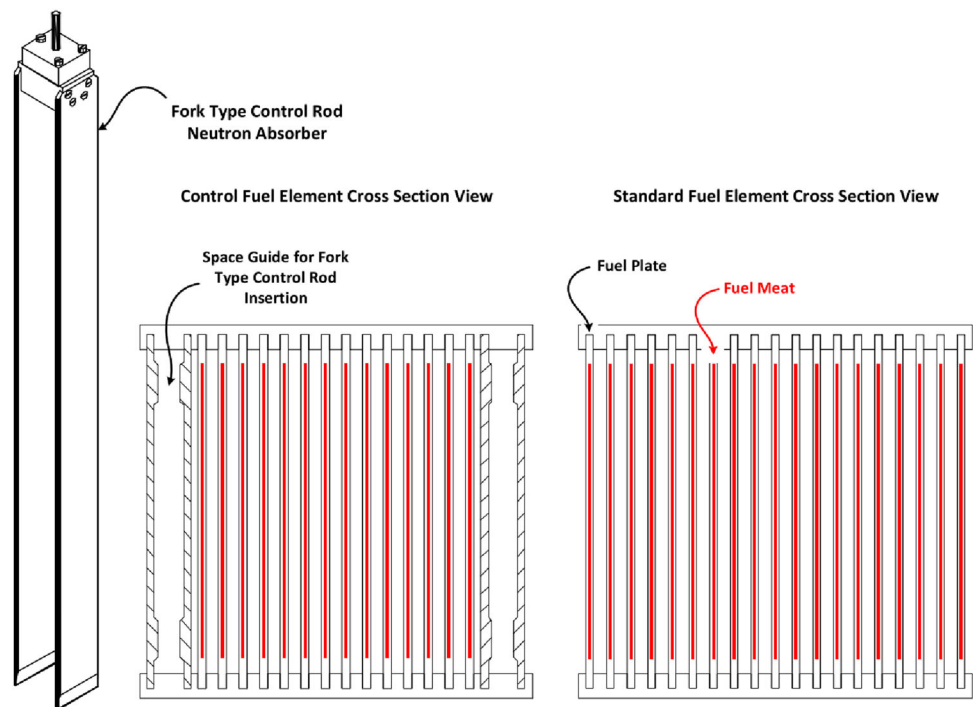1. 2D steady-state neutronics benchmark.

The 2D benchmark TWIGL is used for the code test [18]. The geometric layout of the 1/4 core is shown in

Fig. 1, and the macroscopic cross sections used are listed in Table 1. Both triangular and quadrilateral elements can be used for 2D geometry meshing, and Fig. 2 shows the 2D mesh adopted by the present study. The steady-state neutronic parameters are calculated by FEMN. k_{eff}^* and adjoint flux are shown in Tables 2 and 3 and 4, respectively.

Compared with the reference value [18], the deviation of k_{eff}^* is 0.000002, while the deviation of adjoint flux in the outermost assemblies is less than 4%. The deviation is mainly affected by the mesh size, and it can be further reduced by mesh refinement.

1. 3D steady-state neutronics benchmark.

The 3D benchmark IAEA-3D PWR is used for the code test [19]. A schematic of the 3D benchmark is shown in

Fig. 7 (Color online) First core configuration of the TRR

TRR First Operating Core Configuration

CFE: Control Fuel Element
RR: Regulating Rod
SR: Shim Rod / Safety Rod

Fork Type Neutron Absorbers
SRs: Cd-In-Ag (5%, 15%, 80%)
RR: Stainless Steel

14 Fuel Plates
LEU (20%) U_3O_8Al

SFE: Standard Fuel Element

19 Fuel Plates
LEU (20%) U_3O_8Al

Irradiation Boxes

Light Water as Reflector, Moderator, and Biological Radiation Shield of the Core

Fig. 8 Fork-type control rod and cross-sectional view of the CFE and SFE

Fork Type Control Rod Neutron Absorber

Control Fuel Element Cross Section View

Space Guide for Fork Type Control Rod Insertion

Standard Fuel Element Cross Section View
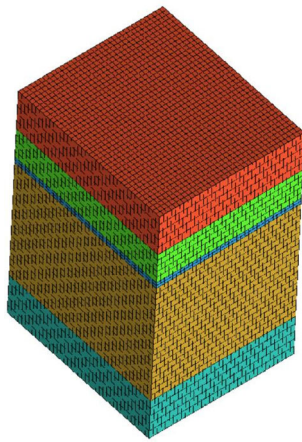
Fuel Plate

Fuel Meat

Fig. 9 (Color online) Meshes used for the TRR benchmark

Fig. 3, and the macroscopic cross sections used are listed in Table 5. Both triangular prism and hexahedral elements can be used for 3D geometric meshing. Figure 4 shows the 3D mesh adopted by the present study. The steady-state neutronic parameters are calculated by FEMN. k_{eff}, k_{eff}^*, and power distribution are shown in Tables 6 and 7.

Compared with the reference value [19], the deviation of k_{eff} is 0.00004. The deviation of heat deposition of the inner fuel assembly is less than 1%. Although the deviation of the outer fuel assembly close to the reflector is high, the overall deviation is less than 2.2%. The deviation is mainly affected by the mesh size, and it can be further reduced by mesh refinement.

The forward flux and adjoint flux can also be adequately determined by FEMN. The distribution of forward flux and adjoint flux for the 3D benchmark is shown in Figs. 5 and 6, respectively.

3 Results and discussion

3.1 Description of the TRR

The TRR is a 5-MW pool-type light-water moderated, heterogeneous solid fuel reactor, in which the water is also used for cooling and shielding. The TRR core is immersed in either section of a two-section, concrete pool filled with water. Utilization of the reactor is essential for research, training, and production of radioisotopes [12]. Substantial research has been performed on the point reactor kinetic parameters of the TRR; thus, it was chosen as a benchmark to facilitate the calculation comparison. The first core configuration of the TRR is shown in Fig. 7 [13].

The standard fuel element (SFE) consists of 19 fuel plates with 20% enrichment of uranium 235. Each fuel plate consists of two unit areas of fuel cladding and one

fuel meat; the meat is made of U3O8 powder dispersed in a pure aluminum matrix, and the cladding and other structural materials are Al6061. The coolant channel is located between the fuel plates. The control fuel element (CFE) consists of 14 fuel plates with 20% enrichment of uranium 235, and each fuel plate consists of two unit areas of fuel cladding and one fuel meat.

The shim safety control rod is composed of two absorbing plates and a knuckle subassembly. The absorber plate is an alloy of silver, indium, and cadmium (80, 15, and 5% wt., respectively), while the regulating rod is made of stainless steel. All absorbing rods are fork type. The main geometrical data of the CFE and SFE can be found in Ref. [12], and the configuration is shown in Fig. 8 [13].

The calculation of TRR's effective point reactor kinematic parameters involves three steps: (1) Preparation of the six-group cross section and six-group neutron velocity by WIMS and 2DSN; (2) Calculation of the six-group forward flux and adjoint flux with the Galerkin finite element method; (3) Calculation of the effective point reactor kinetic parameters. Because the TRR core is asymmetric, the use of triangular prism elements for geometric meshing and six-group calculation will cause substantial memory consumption, which is impractical for personal computers. Therefore, this work uses a memory-saving hexahedron meshing method, and Fig. 9 shows the meshes used in the calculation.

To distinguish the energy spectrum between prompt and delayed neutrons, the total number of energy groups must be greater than two groups, because in a typical two-group structure, neutrons can only be produced in the fast group, so the effect of delayed neutrons is not reflected. The neutron group structure, transient neutron energy spectrum, delayed neutron energy spectrum, and delayed neutron parameters of ^{235}U and ^{238}U can be found in Ref. [12].

3.2 Results and discussion

The steady-state neutronic parameters of the TRR were calculated using the FEMN, and the excess reactivity in this state is 6344 pcm. The forward flux and adjoint flux in the axial plane of 51.5 cm are shown in Figs. 10 and 11, respectively. The forward flux and adjoint flux distribution of the TRR in this state is not given in relevant literature, so only the calculation results are given here for peer reference. For FEMN, the relative error of the steady-state calculation has been discussed, and interested readers can refer to Sect. 2. From the perspective of excess reactivity, the deviation between the calculated value (6344 pcm) and the reference value (6481 pcm) of Ref. [12] is 2%, which proves that the steady-state calculation is reliable from the side.

Fig. 10 (Color online) Distribution of forward flux for the TRR obtained by FEMN ($Z = 51.5$ cm). **a** Forward flux of group 1; **b** Forward flux of group 2; **c** Forward flux of group 3; **d** Forward flux of group 4; **e** Forward flux of group 5; **f** Forward flux of group 6
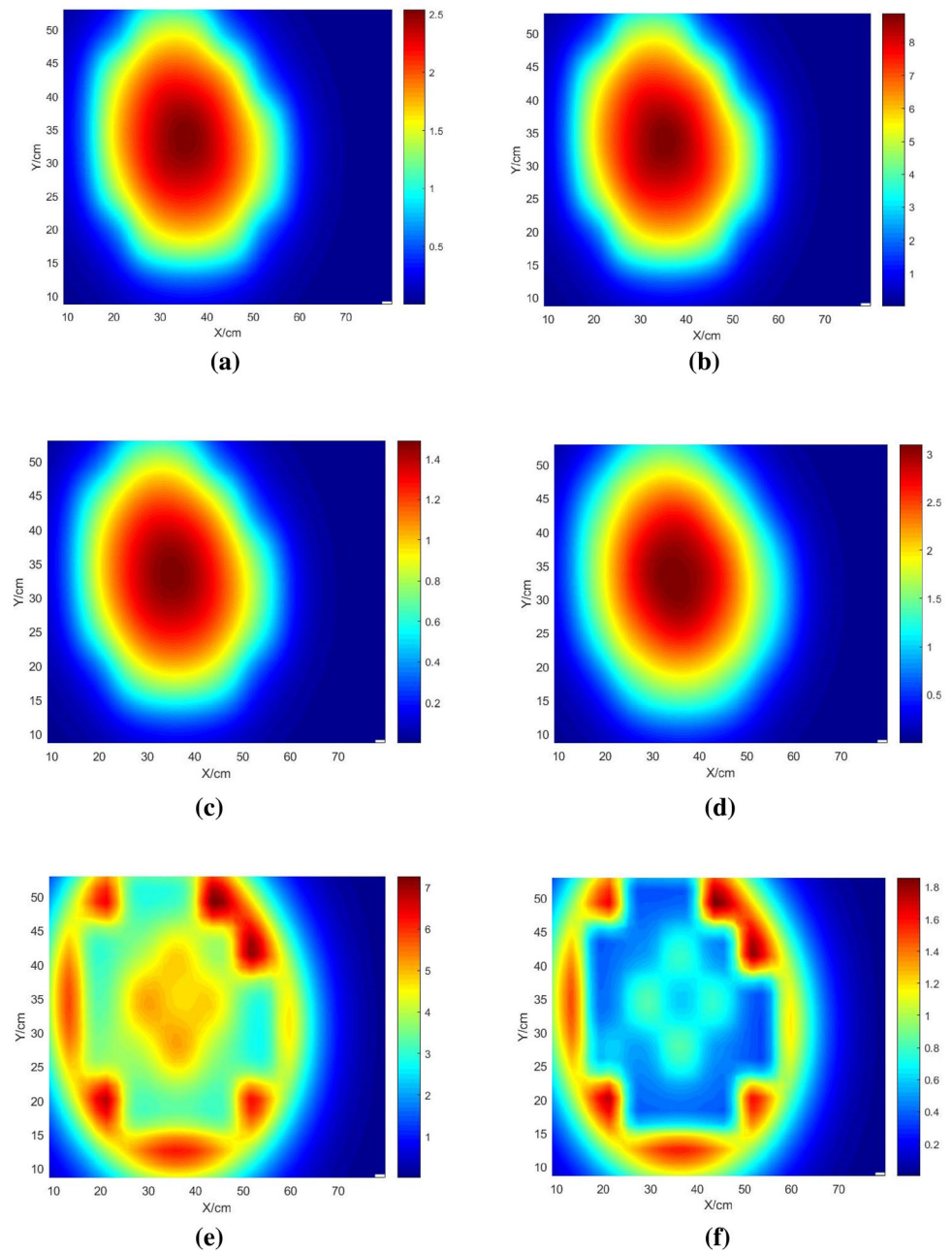
(a)

(b)

(c)

(d)

(e)

(f)

Fig. 11 (Color online) Distribution of adjoint flux for the TRR obtained by FEMN (Z = 51.5 cm). **a** adjoint flux of group 1; **b** adjoint flux of group 2; **c** adjoint flux of group 3; **d** adjoint flux of group 4; **e** adjoint flux of group 5; (f) adjoint flux of group 6
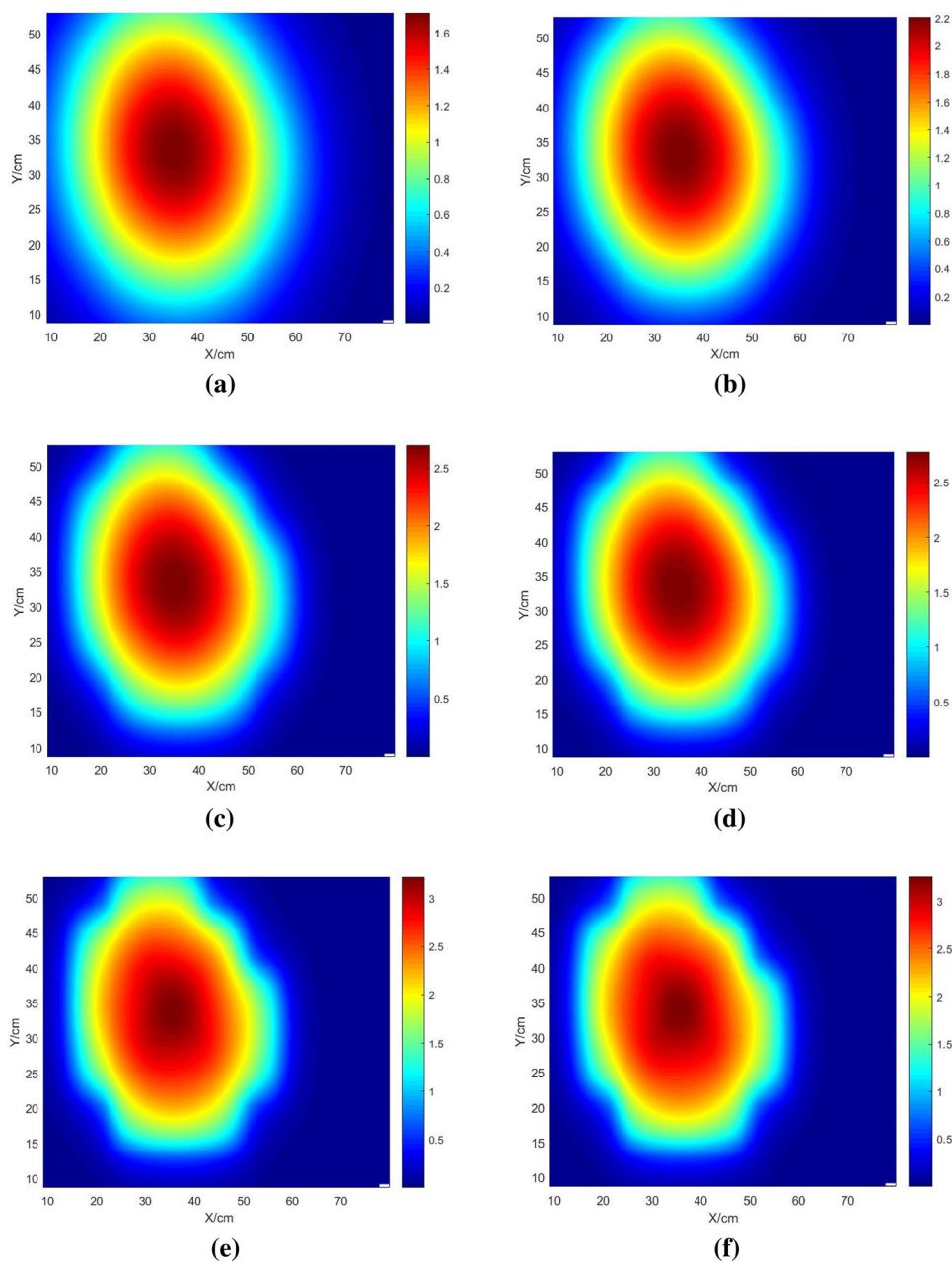

Table 8 Effective point reactor kinetic parameters of the TRR

Item		Value (calculated/recommended [12])
Effective delayed neutron fraction	Group 1	0.00026/0.00024
	Group 2	0.00148/0.00158
	Group 3	0.00133/0.00142
	Group 4	0.00288/0.00286
	Group 5	0.00094/0.00085
	Group 6	0.00020/0.00031
	Total	0.00709/0.00726
Prompt neutron lifetime (μ sec)		43/48

Equations (1) and (2) proposed above are used to process the effective point reactor kinetic parameters of the TRR, and the calculated results are shown in Table 8. Compared with the recommended value of Ref. [12], the relative error of the effective delayed neutron fraction is 2%, while the relative error of the prompt neutron lifetime is 10%. The main reason for the relative error is that the cross sections and neutron energy spectra used by different researchers are inconsistent, which eventually leads to some slight differences in forward flux, adjoint flux, and group neutron velocity.

4 Conclusion

1. Based on the internally developed code FEMN, a method for determining effective point reactor kinetic parameters was developed and validated.

2. Compared with the reference values, the relative errors of the effective delayed neutron fraction and prompt neutron lifetime are 2% and 10%, respectively. The main factor that led to the errors was the inconsistency between the cross sections and the neutron energy spectra.

References

1. A. Hébert, Application of a dual variational formulation to finite element reactor calculations. Ann. Nucl. Energy 20(12), 823–845 (1993). https://doi.org/10.1016/0306-4549(93)90076-2
2. L.A. Semenza, E.E. Lewis, E.C. Rossow, The application of the finite element method to the multigroup neutron diffusion equation. Nucl. Sci. Eng. 47(3), 302–310 (1972). https://doi.org/10.13182/NSE72-A22416
3. Y. Naito, R. Kawamura, Y. Tokuno et al., A computer program for solving the three-dimensional multigroup diffusion equation by finite element method with 20-node isoparametric element (FEM3DJAR). Prog. Nucl. Energy 18(1–2), 207–214 (1986). https://doi.org/10.1016/0149-1970(86)90027-2
4. K. Azekura, New finite element solution technique for neutron diffusion equations. J. Nucl. Sci. Technol. 17(2), 89–97 (1980). https://doi.org/10.1080/18811248.1980.9732552
5. C.Y. Zhang, G. Chen, Fast solution of neutron diffusion problem by reduced basis finite element method. Ann. Nucl. Energy 111, 702–708 (2018). https://doi.org/10.1016/j.anucene.2017.09.044
6. S.A. Hosseini, N. Vosoughi, Neutron noise simulation by GFEM and unstructured triangle elements. Nucl. Eng. Des. 253, 238–258 (2012). https://doi.org/10.1016/j.nucengdes.2012.08.023
7. S.A. Hosseini, F. Saadatian-Derakhshandeh, Galerkin and generalized least squares finite element: a comparative study for multi-group diffusion solvers. Prog. Nucl. Energy. 85, 473–490 (2015). https://doi.org/10.1016/j.pnucene.2015.07.009
8. S.A. Hosseini, Development of galerkin finite element method three-dimensional computational code for the multigroup neutron diffusion equation with unstructured tetrahedron elements. Nucl. Eng. Technol. 48, 43–54 (2016). https://doi.org/10.1016/j.net.2015.10.009
9. S.A. Hosseini, Sensitivity analysis of the Galerkin finite element method neutron diffusion solver to the shape of the elements. Nucl. Eng. Technol. 49, 29–42 (2017). https://doi.org/10.1016/j.net.2016.08.006
10. A.V. Avvakumov, P.N. Vabishchevich, A.O. Vasilev et al., Solution of the neutronics code dynamic benchmark by finite element method. AIP Conf. Proc. 1773, 110003 (2016). https://doi.org/10.1063/1.4965007
11. S. González-Pintor, D. Ginestar, G. Verdú, High order finite element method for the lambda modes problem on hexagonal geometry. Ann. Nucl. Energy 36, 1450–1462 (2009). https://doi.org/10.1016/j.anucene.2009.07.003
12. M.K. Saadi, A. Abbaspour, Effective point kinetic parameters calculation in Tehran research reactor using deterministic and probabilistic methods. Nucl. Sci. Tech. 28, 171 (2017). https://doi.org/10.1007/s41365-017-0323-7
13. M. Arkani, M. Hassanzadeh, S. Khakshournia, Calculation of six-group importance weighted delayed neutron fractions and prompt neutron lifetime of MTR research reactors based on Monte Carlo method. Prog. Nucl. Energ. 88, 352–363 (2016). https://doi.org/10.1016/j.pnucene.2015.12.005
14. A. Lashkari, H. Khalafi, H. Kazeminejad, Effective delayed neutron fraction and prompt neutron lifetime of Tehran research reactor mixed-core. Ann. Nucl. Energy 55, 265–271 (2013). https://doi.org/10.1016/j.anucene.2012.12.001
15. S.A. Hosseini, N. Vosoughi, M.B. Ghofrani et al., Calculation, measurement and sensitivity analysis of kinetic parameters of Tehran research reactor. Ann. Nucl. Energy 37, 463–470 (2010). https://doi.org/10.1016/j.anucene.2010.01.018
16. M. Zaker, Effective delayed neutron fraction and prompt neutron lifetime of Tehran research reactor. Ann. Nucl. Energy 30, 1591–1596 (2003). https://doi.org/10.1016/S0306-4549(03)00081-1
17. B.X Yuan, H. Zeng, W.K Yang et al, Advances in FEMN: the code for nuclear noise analysis based on ICEM-CFD, in Proc. ASME. ICONE26, vol.3: Nuclear Fuel and Material, Reactor Physics, and Transport Theory, V003T02A006, July 22–26, 2018. https://doi.org/10.1115/icone26-81169
18. K.P. Wang, H.C. Wu, L.Z. Cao, The application of the analytic basis function expansion triangular-z nodal method for neutron diffusion calculation. China. Sciencepap. 10(23), 2774–2778 (2015). https://doi.org/10.3969/j.issn.2095-2783.2015.23.017
19. A. Hotta, H. Ninokata, A.J. Baratta, Development of parallel coupling system between three-dimensional nodal kinetic code ENTREE and two-fluid plant simulator TRAC/BF1. J. Nucl. Sci. Technol. 37(10), 840–854 (2000). https://doi.org/10.1080/18811248.2000.9714965